

Single-cell and bulk RNA sequencing data jointly reveals *VDAC2*'s impacts on prognosis and immune landscape of NSCLC

Ying Ma^{1,*}, Bateer Han^{2,*}, Qin Yu³, Nashunbayaer Zha¹, Zhiyuan Deng³, Junguo Liang¹, Rong Yu³

¹Department of Thoracic Surgery, Affiliated Hospital of Inner Mongolia Medical University, Hohhot 010059, Inner Mongolia Autonomous Region, China

²Department of Thoracic Surgery, Peking University Cancer Hospital (Inner Mongolia Campus) and Affiliated Cancer Hospital of Inner Mongolia Medical University, Hohhot 010020, Inner Mongolia Autonomous Region, China

³Department of Radiation Oncology, Peking University Cancer Hospital (Inner Mongolia Campus) and Affiliated Cancer Hospital of Inner Mongolia Medical University, Hohhot 010020, Inner Mongolia Autonomous Region, China

*Equal contribution

Correspondence to: Rong Yu; email: mgyurong@163.com, <https://orcid.org/0009-0008-0816-9587>

Keywords: non-small cell lung cancer, single-cell transcriptome, *VDAC2*, prognosis, immune landscape

Received: June 8, 2023

Accepted: November 20, 2023

Published: February 20, 2024

Copyright: © 2024 Ma et al. This is an open access article distributed under the terms of the [Creative Commons Attribution License](https://creativecommons.org/licenses/by/4.0/) (CC BY 4.0), which permits unrestricted use, distribution, and reproduction in any medium, provided the original author and source are credited.

ABSTRACT

Non-small cell lung cancer (NSCLC) is characterized by stronger metastatic ability and worse prognosis. In NSCLC, hypoxia is a major cause of invasion and metastasis through promoting angiogenesis. In present study, NSCLC cell clusters were extracted from single cell-sequencing dataset GSE131907, which were combined with hypoxia-related genes to group clusters. qRT-PCR and western blot were used to validate the expression of target gene. Nine NSCLC clusters were extracted, which were divided into two hypoxia-related subgroups, C1 and C2. Totally 101 differentially expressed prognostic genes were identified between subgroups. Of which, *VDAC2* showed excellent prognostic value for NSCLC and was selected for further analysis. *VDAC2* was upregulated in tumor samples in TCGA and was correlated with advanced stages. *In vitro* experiments validated this trend. Five crucial immune cells showed differential infiltration proportions between high and low *VDAC2* expression groups. *VDAC2* knockdown significantly inhibited the proliferation and invasion ability of NSCLC cells. Integrating single cell and bulk sequencing data as well as wet lab experiments, hypoxia-related *VDAC2* exhibited important prognostic value and showed the promise of becoming immune-therapy target in NSCLC.

INTRODUCTION

Non-small cell lung cancer (NSCLC), as one of the main subtypes of lung cancer, accounts for 85% of all diagnosed lung cancer cases [1]. The primary subtypes of NSCLC comprise lung adenocarcinoma (LUAD) and lung squamous cell carcinoma (LUSC) [2]. Currently, in patients at stages I and II, the standard treatment of NSCLC is surgical resection followed by adjuvant systemic therapy [3]. In advanced NSCLC patients, the predominant treatment includes immune checkpoint inhibitor (ICI) monotherapy or its combination with chemotherapy [4]. Unfortunately, despite the great development of therapeutic strategies, the 5-year overall

survival (OS) rate of NSCLC is still unsatisfied, approximately only 23% [5]. On the other hand, NSCLC is prone to metastasize at an early stage, especially lymph node metastasis, thus the prognosis of NSCLC is usually suboptimal [6]. Some markers, like PD-L1 expression and tumor mutation burden (TMB), have been applied in clinical lung cancer cases for predicting patients' immunotherapy responses [7], whereas tumor heterogeneity is still a great challenge in clinical practice of cancers. Accordingly, great efforts should be devoted to exploring more details relating to the intratumoral heterogeneity of NSCLC, thereby indirectly conducive to improve the clinical outcome of patients.

Hypoxia is a common micro-environmental trait in most solid tumors, which is caused by an imbalance between tumor cell proliferation and blood oxygen supply [8]. Hypoxia in solid tumors has been linked to cancer patient resistance to chemotherapy and radiation, and it often promotes a more aggressive tumor phenotype, which contributes to poor outcomes of patients [9]. Hypoxia related conditions are increasingly regarded as the critical aspect affecting the malignant progression of lung cancer [10–12]. In NSCLC, long-term moderate hypoxia would elevate the expression of *FGFR1* and maintain the MAPK activation, thereby promoting epidermal growth factor receptor (EGFR) tyrosine kinase inhibitors (TKI) resistance [13]. Chronic intermittent hypoxia can promote lung cancer stem cells-like properties via activating mitochondrial reactive oxygen species (ROS) [14]. Hypoxia induction mediated by hypoxia-inducible factor 2 α (HIF-2 α) increases the epithelial-mesenchymal transition (EMT) events and *NEAT1* expressions in NSCLC under hypoxic condition via regulating miR-101-3p/SOX9/Wnt/ β -catenin signal pathway, promoting the progression of NSCLC [15]. In addition, under hypoxic conditions, cell autophagy involves in improving NSCLC antiradiation capacity by regulating the amount of ROS, negatively affecting radiotherapy efficacy and leading to a poor prognosis of lung cancer patients [16]. In short, hypoxia can promote the NSCLC cell progression and chemoresistance. However, more detailed hypoxia related functions in heterogeneous NSCLC cells still lack clear clarification as far as we know.

Herein, in this study, the NSCLC related single-cell and bulk RNA sequencing data have been comprehensively analyzed in order to decipher more details involving the tumor microenvironment (TME) and intratumoral heterogeneity basing on hypoxia related genes. Our findings are promising to give more insights into understanding tumor as well as immune microenvironment of NSCLC patients.

RESULTS

Identification of heterogeneous NSCLC cell subpopulations

To better understand the intratumoral heterogeneity of NSCLC and hypoxia from distinct levels, our present work was conducted according to the flow chart in Figure 1. We firstly analyzed the sc-RNA sequencing data to identify the heterogeneous cell subsets. In GSE131907 dataset, we processed the samples with Seurat R package, and selected the top 15 principal components among all clusters (Figure 2A). The cells were annotated into 19 cell clusters by Umap (Uniform Manifold Approximation and Projection) method (Figure 2B). Subsequently, the LUAD

marker genes *NAPSA*, *NKX2-1*, the LUSC marker genes *TP63*, *KRT5*, as well as *EPCAM* and *MET* were adopted to identify the cancer cell clusters. We found that cluster4, cluster6, cluster11, cluster12 and cluster16 belonged to cancer cell populations (Figure 2C). To screen the tumor cells more accurately, these 5 cancer cell clusters were analyzed following the above process again, and totally 16 cell clusters were obtained (Figure 2D, 2E). Finally, cluster0, cluster3, cluster4, cluster6, cluster8, cluster10, cluster13, cluster14, cluster15 were identified as the NSCLC cell populations by further cancer cell annotation (Figure 2F).

Definition of different hypoxia related NSCLC subpopulations - C1 and C2 groups

Next, we analyzed the marker genes' functional information of the above 9 cell subsets to better understand the potential functional ways. The marker genes of cluster0, cluster4 and cluster10 were significantly enriched in 9, 7 and 6 KEGG pathways, respectively, and the marker genes of other clusters were enriched in 20 KEGG pathways (Supplementary Figures 1, 2). In addition, the marker genes of these 9 clusters were significantly enriched in 20 GO terms, respectively (Supplementary Figures 3, 4). We noticed that most of the functional terms involved in multiple critical processes and aspects in tumorigenesis, such as MAPK signaling pathway and HIF-1 signaling pathway, which implied the distinct function of heterogeneous cell subsets in NSCLC.

Hypoxic conditions in TME are considered as a driver of tumor malignancy in NSCLC [10]. To better decipher hypoxic impacts on tumor cells in TME, we performed the cross-over analysis between hypoxia related genes (HRGs) and marker genes of these cluster. The significantly differential HRG expression pattern was observed between cluster0, cluster3 and cluster4, cluster6, cluster8, cluster10, cluster13, cluster14 (Figure 3). Therefore, according to the HRG expression, the cluster0 and cluster3 were then defined as C1 group, and cluster4, cluster6, cluster8, cluster10, cluster13, cluster14 were classified as C2 group. The samples in C1 and C2 groups were considered distinct hypoxia related heterogeneous NSCLC subpopulations.

Hypoxia heterogeneous NSCLC subpopulation related *VDAC2* showed important prognostic value in NSCLC

Among the marker genes in the hypoxia-related heterogeneous NSCLC subpopulations, C1 and C2, 101 genes were identified to be associated with prognosis of patients by univariate Cox regression analysis (Supplementary Table 1). Of these 101 genes, there

were 11 genes with HR greater than 1, as risk factors for NSCLC (Figure 4A and Supplementary Table 1). Except for *ASPH*, *MT2A* (Supplementary Figure 5A, 5B), the other 9 genes' high expressions were significantly correlated with a poor prognosis of NSCLC patients (Figure 4B–4J). Basing on the KM plotter (<http://kmplot.com/>) database, the *VDAC2* high expression was significantly associated with inferior prognosis of 2437 NSCLC patients among these 9 genes

(Figure 4K). *VDAC2* expression exhibited significantly positive correlation with HIF-1 α (Supplementary Figure 5C). Moreover, the time dependent receiver operating characteristic (ROC) indicated that area under the curve (AUC) values of *VDAC2* in 3 years and 5 years were over 0.70, and the AUC value of *VDAC2* in 7 years was 0.629 (Figure 4L), indicating *VDAC2* had better diagnostic value for NSCLC. Therefore, *VDAC2* was selected for our subsequent analysis.

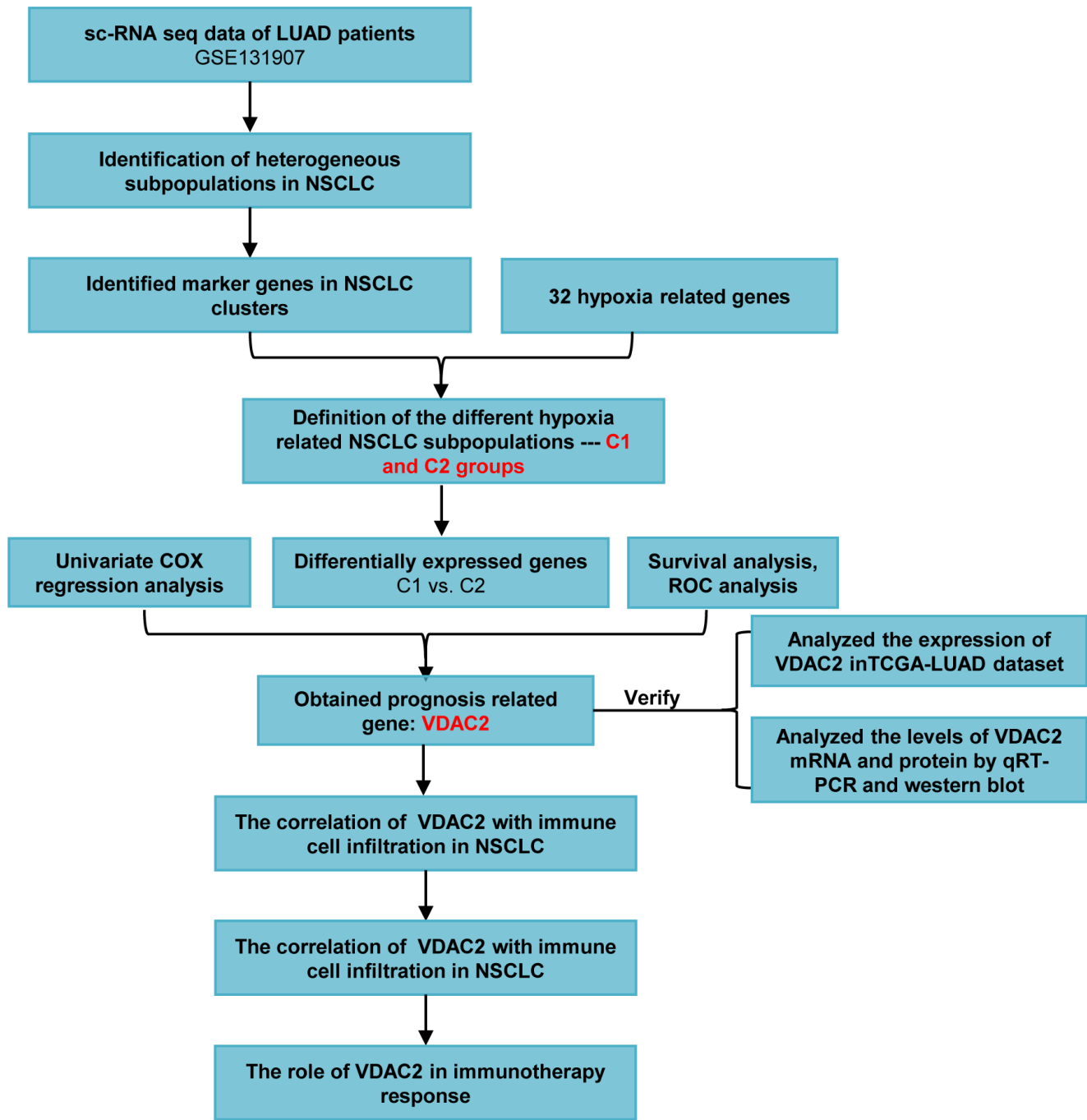


Figure 1. The flow chart of this study.

VDAC2 was highly expressed in NSCLC

In the TCGA-LUAD dataset, we found that the *VDAC2* was significantly highly expressed in cancer samples comparing to adjacent samples (Figure 5A, cancer vs. normal). A similar high expression of *VDAC2* protein was also observed in tumor tissue samples of NSCLC from Human Protein Atlas (HPA, <https://www.proteinatlas.org/>) database (Figure 5B). Furthermore, the expression of *VDAC2* was significantly increased in stage IV patients comparing to stage I and stage II patients (Figure 5C).

To validate the *VDAC2* expression in NSCLC using wet lab tools, we analyzed the expression of *VDAC2* in NSCLC clinical samples and cell lines. The levels of *VDAC2* mRNA and protein were increased in NSCLC tissue comparing to normal tissue (Figure 5D, 5E). Immunofluorescence results showed that *VDAC2* protein expression was significantly increased in lung cancer tissues compared to adjacent noncancerous tissues (Figure 5F). Moreover, *VDAC2* mRNA and

protein were also highly expressed in A549 and NCI-H1299 cells compared to HBE cells (Figure 5G, 5H). Collectively, the aberrant expression of *VDAC2* might show tumor promoting role in NSCLC.

The correlation between *VDAC2* and immune landscape in NSCLC

The samples in TCGA-LUAD dataset were split into high and low *VDAC2* expression groups according to the median value of *VDAC2* expression. Firstly, the immune score and stromal score were decreased in high *VDAC2* expression group (Figure 6A, 6B). In addition, comparing to low *VDAC2* expression group, the relative infiltrating proportions of B cells naïve, T cells CD4 memory resting, Mast cells resting were reduced in high *VDAC2* expression group, and the Macrophages M0, Dendritic cells activated were increased (Figure 6C, 6D). Among all differentially infiltrated immune cells, the correlation analysis indicated that the T cells CD8 had strong negative correlation with T cells CD4 memory resting in NSCLC (Figure 6E).

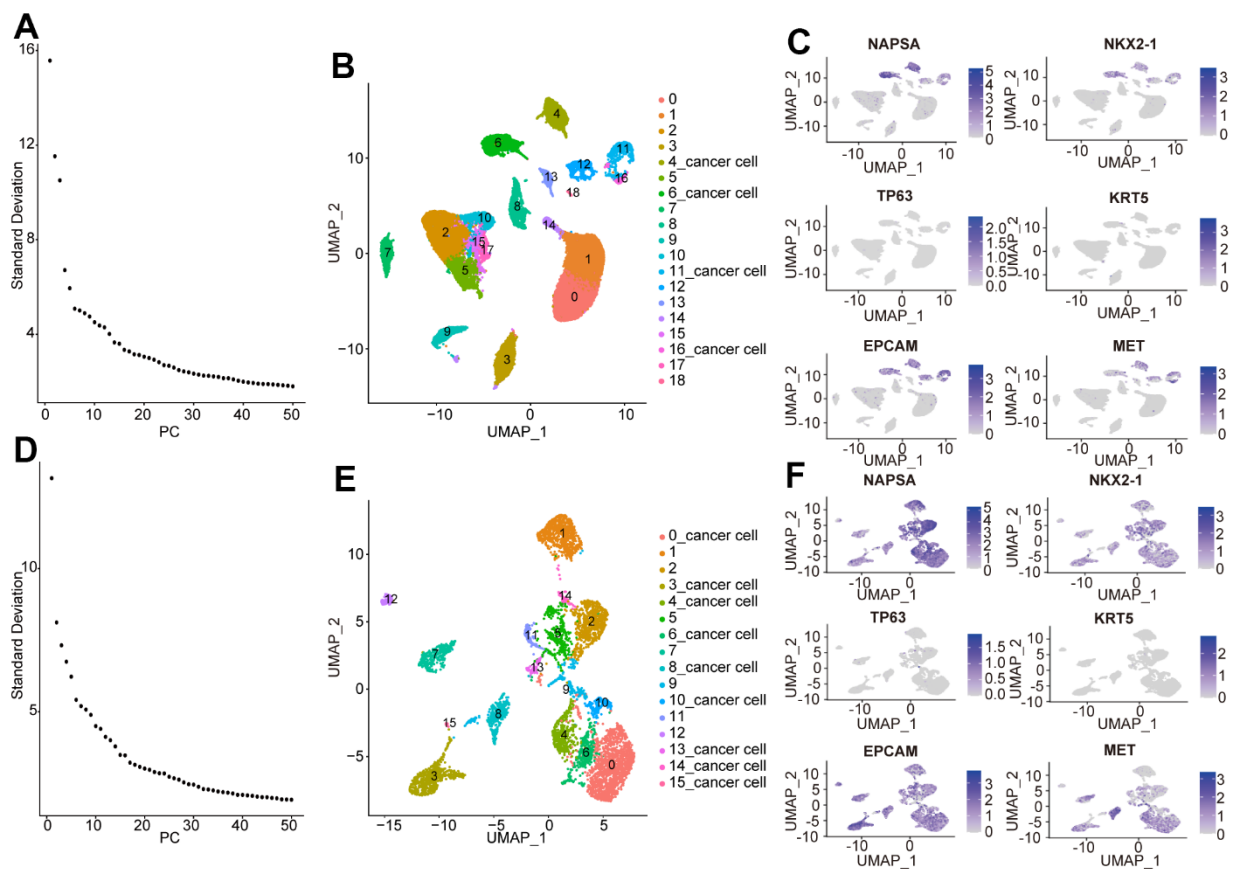


Figure 2. Identification of heterogeneous NSCLC cell subpopulations. (A) First principal component score, (B) The cells were annotated into 19 cell clusters by Umap in NSCLC. (C) Identified NSCLC clusters using marker genes of cancer. (D) Second principal component score. (E) The NSCLC cell populations were annotated into 16 cell clusters by Umap. (F) Identification of NSCLC cluster by cancer cell marker gene.

NSCLC patients' clinical responses with distinct *VDAC2* expression

Subsequently, we analyzed the somatic mutation status in high and low *VDAC2* expression groups, and calculated the TMB. The *TP53* and *TTN* were more frequently mutated in high *VDAC2* expression group than in low expression group (Figure 7A). In addition, the TMB was significantly increased in

high *VDAC2* expression group (Figure 7B, 7C). Critical immune checkpoints PD-1 (*PDCD1*), PD-L1 (*CD274*), PD-L2 (*PDCD1LG2*), *CD80*, *CD86* were significantly upregulated in high *VDAC2* expression group (Figure 7D). The immune checkpoints *CCL2*, *IL1A*, *LAP3* and *TGFB1* expressions were significantly increased in high *VDAC2* group, whereas *KLRB1* expression was decreased (Figure 7E, high vs. low).



Figure 3. The heatmap of differential expression of hypoxia related marker genes in all cell clusters.

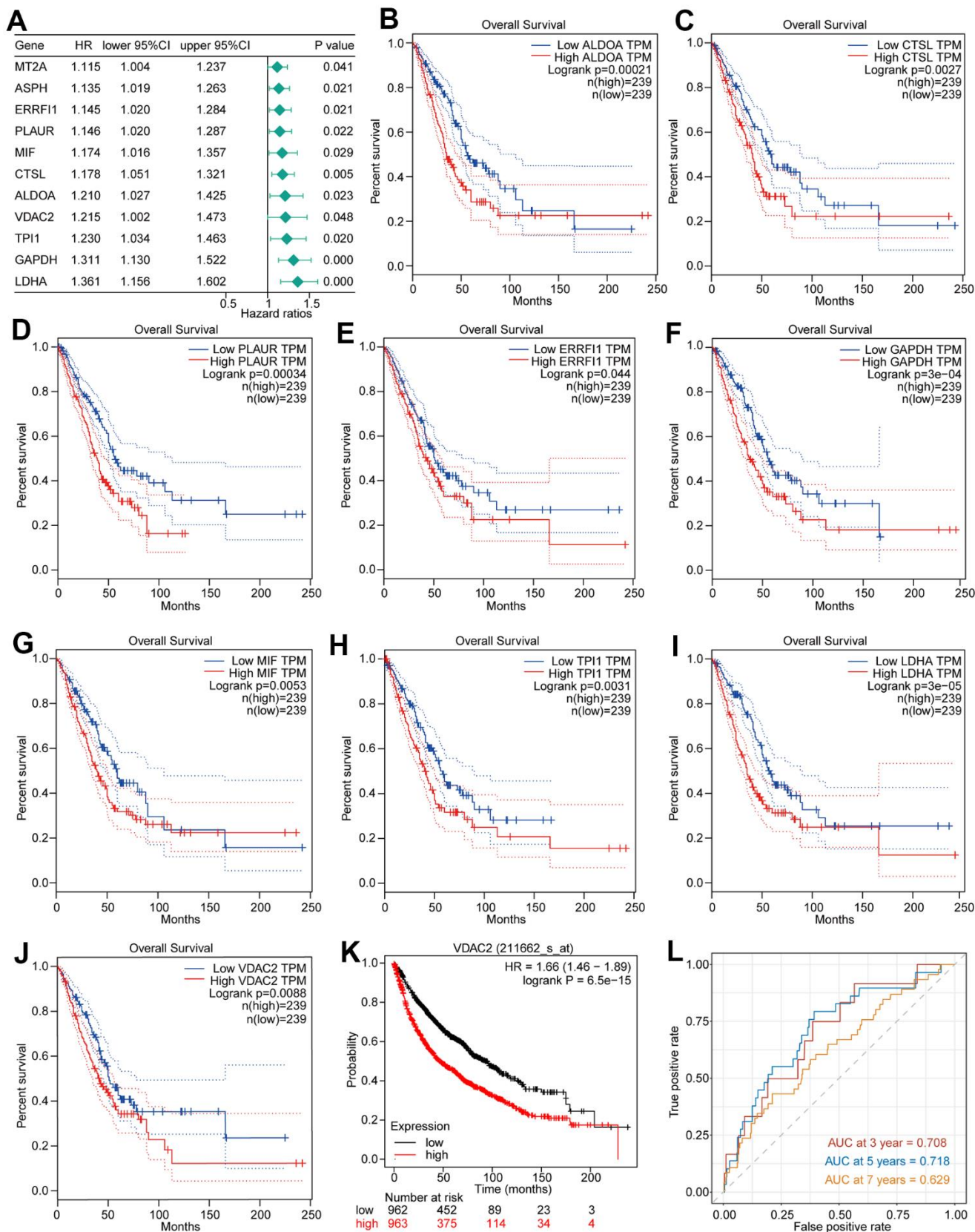


Figure 4. Hypoxia heterogeneous NSCLC subpopulation related genes' prognostic value in NSCLC. (A) The 11 prognosis related genes with HR greater than 1. (B–J) The Kaplan Meier survival curves of 9 genes expression (high and low) in the TCGA-LUAD dataset. (K) The results of Kaplan Meier survival analysis of *VDAC2* in the 2437 NSCLC patients. (L) Time dependent ROC curves of *VDAC2* in NSCLC.

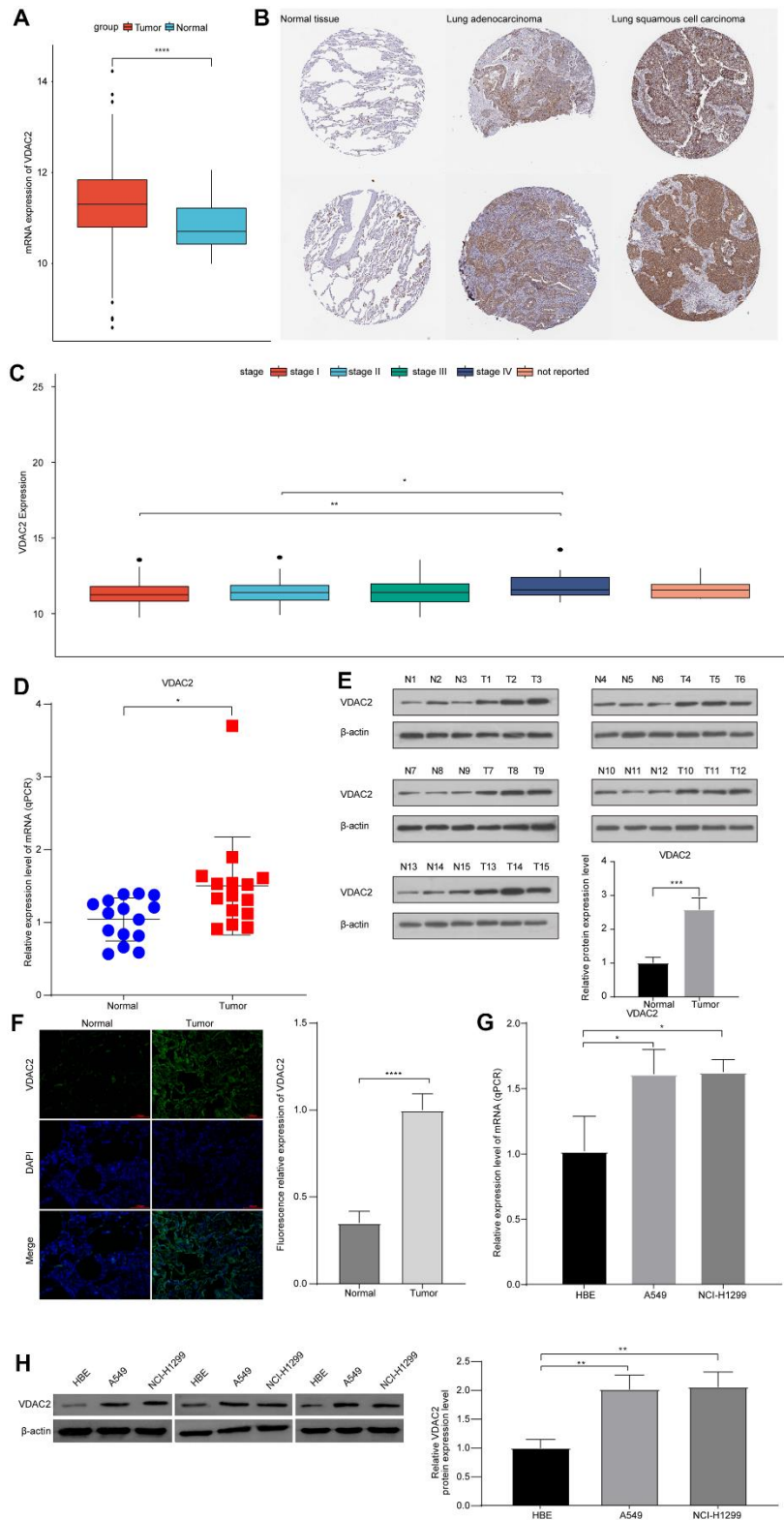


Figure 5. Hypoxia heterogeneous NSCLC subpopulation related VDAC2 showed important prognostic value and tumor promoting role in NSCLC. (A) The expression of VDAC2 in normal and cancer samples basing on TCGA-LUAD cohort. (B) The expression of VDAC2 in NSCLC tissues and normal tissues basing on Human protein atlas database. (C) The expression of VDAC2 in different stages of NSCLC patients. (D, E) The levels of VDAC2 mRNA and protein in clinical NSCLC tissues. (F) The expression of VDAC2 in lung cancer and adjacent noncancerous tissues was detected by immunofluorescence. (G, H) The levels of VDAC2 mRNA and protein expression in A549 and NCI-H1299 cells. * $p < 0.05$, ** $p < 0.01$, **** $p < 0.0001$.

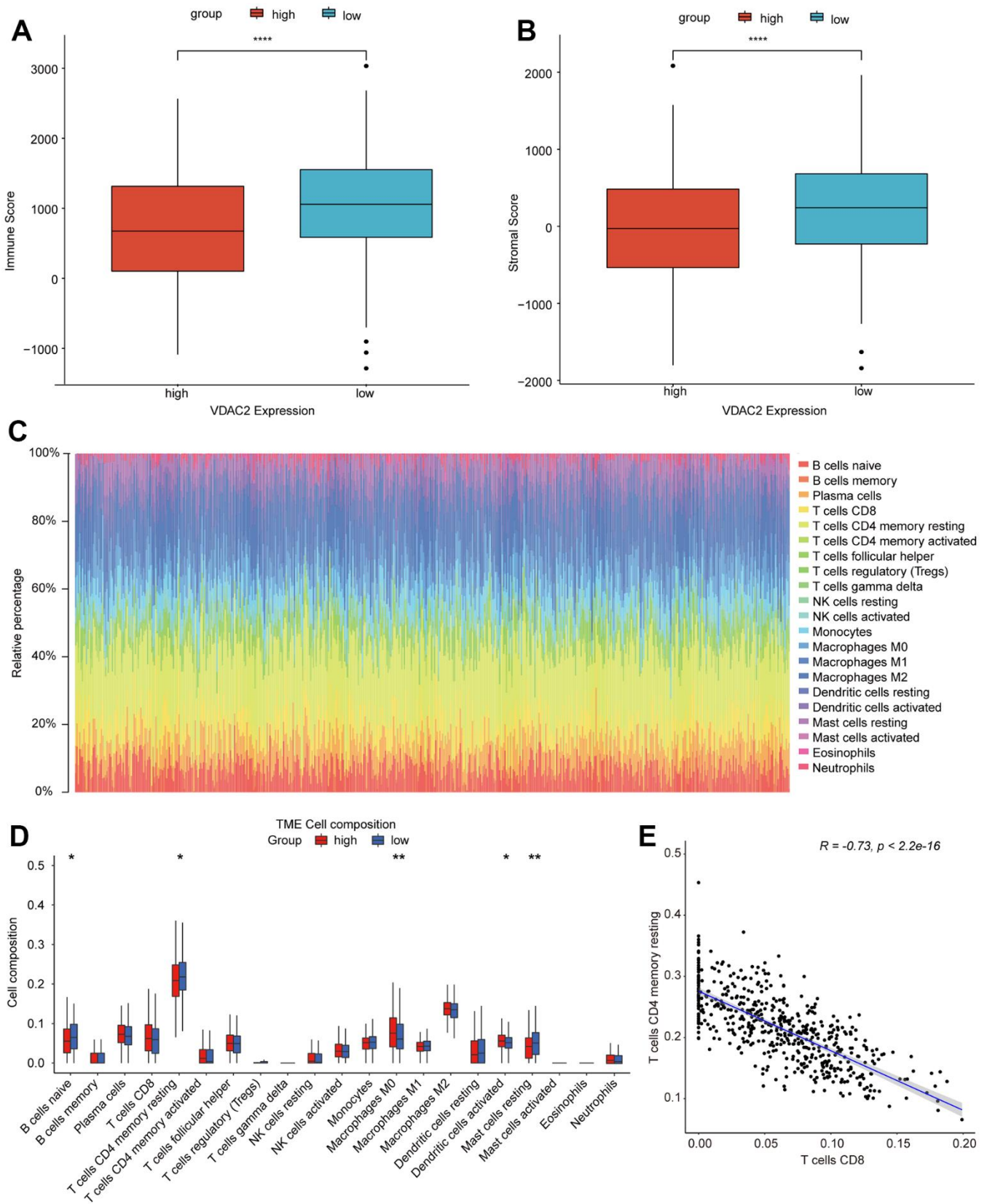


Figure 6. The correlation between VDAC2 and tumor microenvironment in NSCLC. (A, B) The stromal score (A) and immune score (B) between high and low VDAC2 expression groups. (C, D) The correlation of VDAC2 with immune cells infiltration. (E) The correlation between T cells CD8 and T cells CD4 memory resting in NSCLC. * $p < 0.05$, ** $p < 0.01$; *** $p < 0.001$, **** $p < 0.0001$.

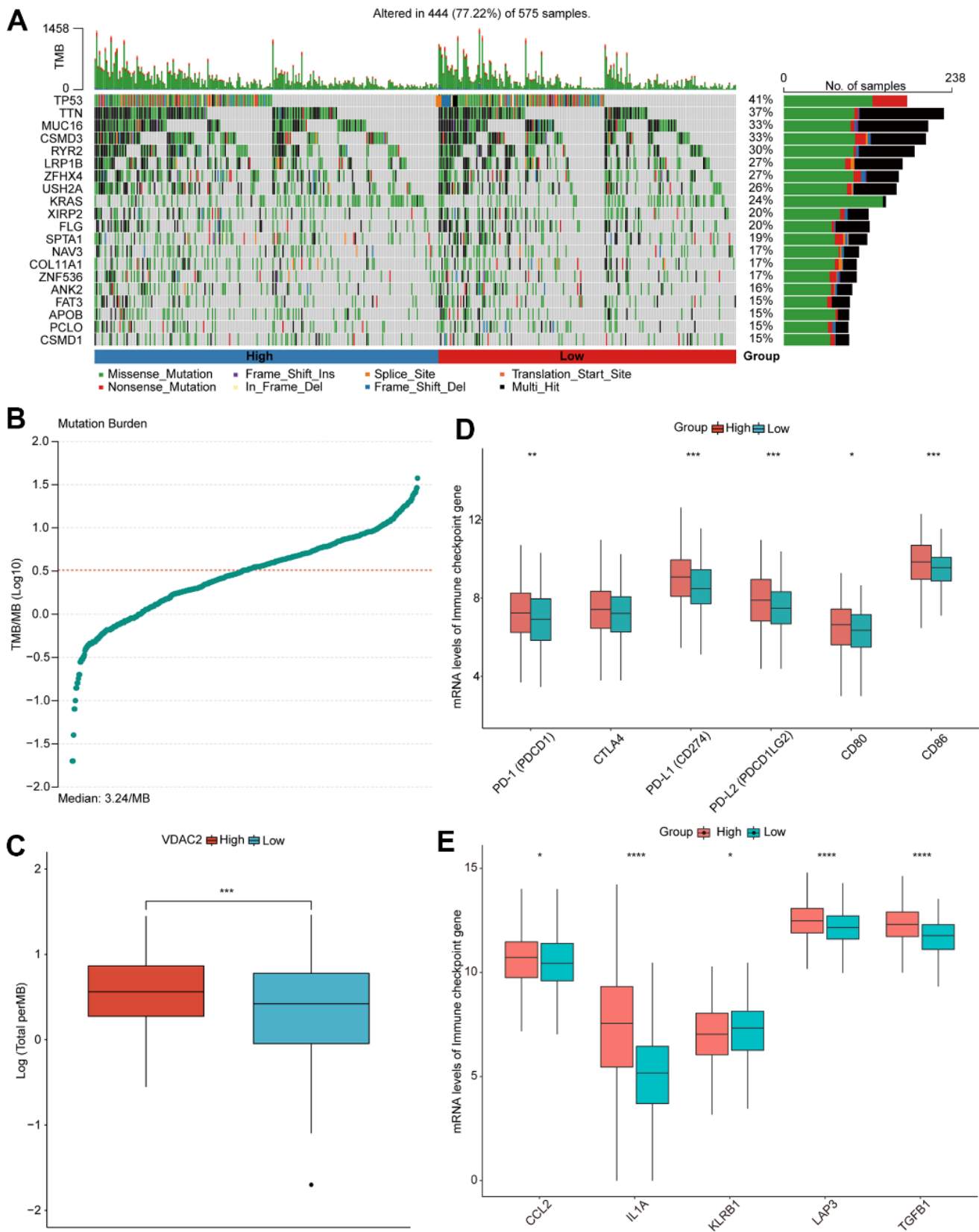


Figure 7. NSCLC patients with distinct *VDAC2* expression exhibited different clinical responses. (A) The waterfall plot of somatic mutation. (B, C) The level of TMB in high and low *VDAC2* expression groups. (D, E) The expression of immune checkpoints in high and low *VDAC2* expression groups. * $p < 0.05$, ** $p < 0.01$; *** $p < 0.001$.

Suppression of *VDAC2* expression might inhibit proliferation and invasion of NSCLC cells *in vitro*

To further decipher the effects of *VDAC2* on progression of NSCLC, we constructed the *VDAC2* knockdown (si-*VDAC2*) A549 cells, and investigated the effects of *VDAC2* underexpression on proliferation and invasion of NSCLC cells. The levels of *VDAC2* mRNA and protein expressions were significantly decreased in A549-si-*VDAC2* group compared to A549-si-NC group (Figure 8A, 8B). The CCK-8 assay showed that knockdown of *VDAC2* significantly inhibited the viability of A549 cells compared to empty vector group (si-NC) (Figure 8C). The results from the clonogenic assay were consistent with the CCK-8 assay data, suggesting that suppression of *VDAC2* expression

inhibited proliferation of A549 cells (Figure 8D). In addition, the result of the transwell assay showed that knockdown of *VDAC2* could attenuate the invasion ability of A549 cells (Figure 8E). These results indicated that *VDAC2* knockdown could inhibit proliferation and invasion ability of NSCLC cells *in vitro*.

DISCUSSION

In this study, we identified nine clusters as NSCLC cell populations by cancer cell identification and signature analysis. Moreover, according to the hypoxia related genes' expression, these clusters were divided into two subgroups (C1 and C2). Totally 101 marker genes of C1 and C2 groups were significantly associated with prognosis of NSCLC patients. Of these 101 genes, high

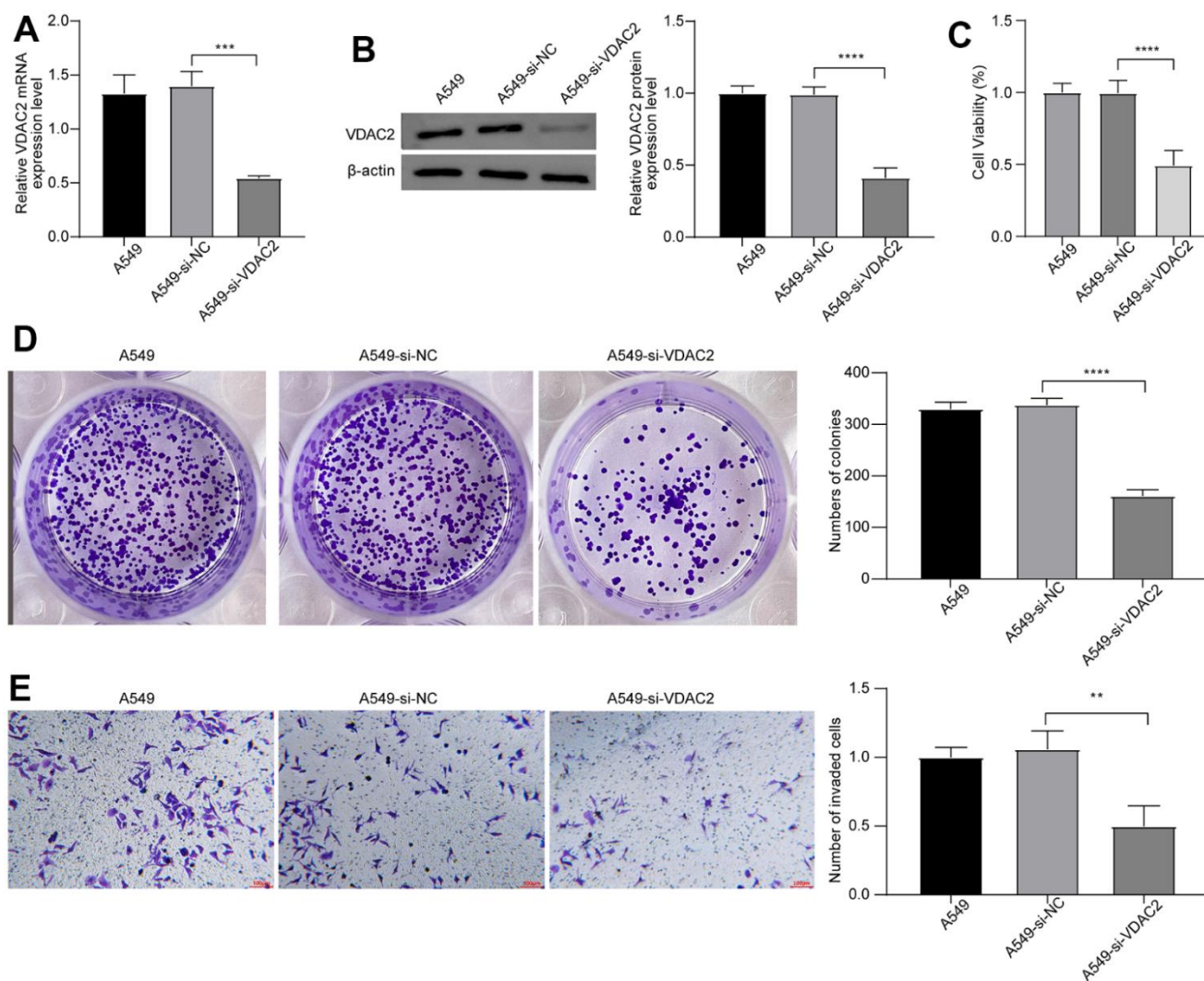


Figure 8. Suppression of *VDAC2* expression might inhibit proliferation and invasion of NSCLC *in vitro*. The levels of *VDAC2* mRNA expression (A) and protein expression (B) in A549-si-*VDAC2* group detected via qPCR and western blot. (C) Cell viability was measured by CCK8 assay. (D) Cell proliferation was detected by clonogenic assay. (E) Invasion ability of cells was detected via transwell assay. ** $p < 0.01$; *** $p < 0.001$, **** $p < 0.0001$.

VDAC2 expression was significantly associated with inferior prognosis of 2437 NSCLC patients, meanwhile *VDAC2* exhibited tumor promoting potential in NSCLC. *VDAC2* is one of the isoforms of Voltage Dependent Anion Channel (VDAC), and it has been proved to be ubiquitously expressing in mammalian [17]. VDAC exists in three isoforms, *VDAC1*, *VDAC2* and *VDAC3* [18]. It has been demonstrated that VDAC plays important role in regulating mitochondrial metabolism and energy functions, and it is involved in apoptotic machinery [16, 19]. Józwiak et al. have revealed that the high level of *VDAC2* protein indicated a poor prognosis of endometrial cancer patients [20], which was consistent with our findings that NSCLC patients with overexpression of *VDAC2* had worse prognosis. We also found that higher *VDAC2* expression was correlated with advanced NSCLC stages. However, Zhou et al. have demonstrated that the patients with *VDAC2* overexpression had better prognosis in glioma, and the *VDAC2* expression was inversely correlated with grades [21]. The above evidences showed that *VDAC2* probably exhibited distinct functions in different cancer types. In addition, *VDAC2* plays a critical role in regulating BAX mediated apoptosis [22]. Wang et al. have reported that the knockdown of *VDAC2* increased the mitochondrial membrane potential and total ROS levels in pancreatic ductal adenocarcinoma cells, and *VDAC2* knockdown potentiated the apoptosis induced by chemotherapy [23]. In melanoma cells, the *FOXMI* could inhibit ferroptosis via regulating the expression of *Nedd4* and the degradation of *VDAC2/3* [24]. In this study, we found that *VDAC2* knockdown significantly inhibited the proliferation and invasion ability of NSCLC cells *in vitro*. However, more details involving how *VDAC2* regulated the malignant cell events in NSCLC deserved further illustration in our future work.

Additionally, the relative proportions of B cells naïve, T cells CD4 memory resting, Mast cells resting were reduced in high *VDAC2* expression group, and the Macrophages M0, Dendritic cells activated were increased. These results indicated that the B cells naïve, T cells CD4 memory resting and Mast cells resting were associated with better prognosis of NSCLC patients, and Macrophages M0, Dendritic cells activated were correlated with poor prognosis. B cells and T cells were integral part of tumor infiltrating lymphocytes. In addition, the T cells predominated in lung cancer immune landscape, and CD4+ T cells and CD8+ T cells were the common prevalent T cell subtypes [25]. The high levels of CD3+ and CD8+ T cells have been implied to correlate with longer survival rate of NSCLC patients [26], and the NSCLC patients with higher CD8(+) counts had longer OS rate [27]. These evidences suggested that the higher CD8(+) infiltration

had better prognostic value in lung cancer, while it was not observed in our present analysis. In addition, Gentles et al. have found that the inactivated mast cells and inactivated CD4 memory T cells were strongly correlated with better prognosis of LUAD patients [28], which indirectly supported our results. In addition, dendritic cells belong to a heterogeneous population of leukocytes that present tumor antigens to antigen-specific helper and cytotoxic T cells [29]. Got et al. have revealed that the mature dendritic cells high density exhibited a strong T cell infiltration in NSCLC patients, and the density of mature dendritic cells was associated with the expression of T-cell activation related genes [30]. They also found that the elevated density of dendritic cells was associated with longer survival rate of NSCLC patients. Accordingly, we hypothesized that the high *VDAC2* expression might be involved in the immune cell infiltration, whereby contributing to the worse prognosis of NSCLC patients.

We also found that the TMB was significantly increased in high *VDAC2* expression group. TMB is a measure of the total number of mutations per coding area of tumor genome, which has been reported to be correlated with the objective response rate to immunotherapy (PD-1 inhibitors) [31]. Previous studies have documented that the high TMB and PD-L1 expression were correlated with better benefit from immune checkpoint blockade treatment in NSCLC patients [32, 33]. Of note, we found that the *PD-1*, *PD-L1*, *PD-L2*, *CD80*, *CD86* were upregulated in high *VDAC2* expression group. Above data suggested that the *VDAC2* expression was indirectly associated with TMB status and immune checkpoint expressions in NSCLC patients, which provided important reference for immunotherapy of NSCLC.

Although our study identified different hypoxia related NSCLC subpopulations - C1 and C2 groups, and obtained a prognosis-related gene *VDAC2* in NSCLC, certain limitations should be noted. On the one hand, the correlation of *VDAC2* expression and cell hypoxia in NSCLC needs further investigations via hypoxia related cell experiments. On the other hand, the NSCLC patients' clinical responses with distinct *VDAC2* expression should be validated in clinical trial cohort, which would further strengthen the clinical predictive value of *VDAC2* in NSCLC.

In summary, basing on hypoxia related heterogeneous NSCLC subpopulations, the prognostic value of *VDAC2* in NSCLC was demonstrated in our work for the first time, integrating single cell sequencing data, bulk sequencing data, and wet lab experiments. High *VDAC2* expression was an unfavorable prognostic indicator for

NSCLC patients, which was profoundly correlated with TMB and immune checkpoints in NSCLC patients. Our findings are expected to provide more reference for the clinical management of patients.

MATERIALS AND METHODS

Data collection

The single-cell RNA sequencing (sc-RNA seq) GSE131907 dataset was collected from Gene Expression Omnibus (GEO, <https://www.ncbi.nlm.nih.gov/geo/>) database. This dataset included 58 clinical samples (comprising 15 lung tumor samples, 5 pleural fluid samples, normal samples and other tissue samples) of 44 LUAD patients. The mRNA expression profiles and somatic mutation data of 513 samples were downloaded from The Cancer Genome Atlas (TCGA, <https://tcga-data.nci.nih.gov/tcga/>) database. Of these 513 samples, totally 500 samples had complete survival information. In addition, the immunohistochemical data of target gene in NSCLC were obtained from the Human Protein Atlas (HPA, <https://www.proteinatlas.org/>) database.

Sample source

Totally 15 NSCLC tissues and 15 normal tissues were obtained from the Affiliated People's Hospital of Inner Mongolia Medical University. All experiments were approved by the ethics committee of the Affiliated People's Hospital of Inner Mongolia Medical University (ethic code: No. WZ202307), conformed to the declaration of Helsinki, and informed consent was obtained from all subjects. The information of patients was shown in Supplementary Table 2.

Identification of heterogeneous subpopulations in NSCLC

The R package “Seurat” was used for filtering out low-quality cells, data normalization, data dimension reduction and other processing of sc-RNA sequencing data in GSE131907 dataset. Then, the cancer cell populations were extracted and further processed again, and all tumor cells were divided into distinct cell clusters.

Identification of hypoxia related NSCLC subpopulation

All of the obtained tumor cell subsets underwent the marker gene annotation, with $p < 0.05$ as a screening criterion. The marker genes were subjected to Gene ontology (GO) and Kyoto Encyclopedia of Genes and Genomes (KEGG) enrichment analysis by R (version 4.2.0, the same below) package “clusterProfiler”. The enriched pathways were selected using $p < 0.05$.

Moreover, we had also downloaded 32 HRG from gene set enrichment analysis (GSEA) database (<https://www.gsea-msigdb.org/gsea/index.jsp>). A cross analysis was then conducted between the marker genes and the HRGs to obtain the candidate genes.

Screening of prognostic candidate genes

Based on the expressions of marker genes and HRGs, the cell clusters were split into C1 and C2 groups. The differentially expressed genes (DEGs) between these two groups were screened using R language package limma, based on $|\text{Log}_2\text{FC}| > 0.5$ and $\text{FDR} < 0.05$. The obtained DEGs were subjected to univariate Cox regression and survival analysis, to further optimize the candidate genes. The survival analysis was conducted using Kaplan-Meier method. Time dependent receiver operating characteristic (ROC) analysis was used to predict the prognostic value of hub gene, in timeROC package of R language.

Gene expression analysis

Gene expression matrix of LUAD samples (TCGA-LUAD.htseq_counts.tsv.gz) were downloaded from the GDC TCGA-LUAD cohort. This matrix included the expression values of *VDAC2*. Subsequently, the Wilcoxon rank sum test was used to compare the expression of *VDAC2* in different groups. $P < 0.05$ is considered statistically significant.

Immune cell infiltration analysis

Estimation of STromal and immune cells in Malignant Tumour tissues using Expression data (ESTIMATE) (<https://R-Forge.R-project.org/projects/estimate/>) function package inferred the proportion or abundance of tumor cells, infiltrating immune cells and stromal cells using transcriptional profiles of cancer samples to calculate the stromal score and immune score of the tumor tissues [34]. The TMB was calculated using R package “maftools”. The infiltration proportions of 22 kinds of immune cells between two groups were analyzed using CIBERSORT [35]. CIBERSORT investigators first designed and validated a leukocyte gene signature set LM22 comprising 574 genes that could distinguish 22 hematopoietic phenotypes, including 7 types of T cell, Naïve and memory B cell, plasma cell, NK cell, and myeloid subsets. The relative proportions corresponding to the 22 immune cells were calculated by deconvolution algorithm based on LM22 pair tissue RNA sequencing data.

Cell culture

The cell lines used in this study included human bronchial epithelial like HBE cells, human NSCLC cells A549 and NCI-H1299. All cells were purchased from Hunan

Fenghui Biological Co., Ltd. (Hunan, China). The HBE, A549 and NCI-H1299 cells were cultured in DMEM medium (Gibco, C11995500BT), Ham's F-12K medium (Gibco, 21127030) and RPMI Medium 1640 medium (GIBCO, C11875500BT), respectively. All mediums were supplemented with 10% fetal bovine serum (GIBCO, 10270-106) and penicillin streptomycin mix (Solarbio, p1400), and placed in 37° C incubator with 5% CO₂.

qRT-PCR assay

The total RNA was extracted with Redzol Reagent (SBS, FTR-50). Reverse transcription was performed with a reverse transcription Kit (GeneCopeia, QP056). The PCR amplification was performed with 2 × SYBR Green qPCR Master Mix (None Rox) (Servicebio, Mpc2203026) in an iQ5 Real-Time PCR amplicon (Applied Biosystems). The primer sequences were displayed in Table 1. The program was as follows: 40 cycles at 95° C for 30 s, 95° C for 15 s, 60° C for 30 s. The internal reference was *β-actin*. mRNA expression levels were determined with 2^{-ΔΔCT} formula.

Western blot assay

The protein was extracted using RIPA lysis solution (Beijing Solarbio Technology Co., Cat # R002) and PMSF solution. The western blot was consistent with previous methods [36]. The first antibodies included VDAC2 (9412, 1: 1000, Cell signaling technology), *β-actin* (ab8226, 1: 1000, Abcam). The second antibody was HRP-labeled Goat anti-rabbit IgG (ab7090, 1: 8000, Abcam). The gray values of the bands were analyzed using ImageJ software.

Immunofluorescence assay

The lung cancer tissues and adjacent normal tissues were collected to make paraffin sections. The paraffin sections were put into sodium citrate antigen retrieval solution and placed in a microwave oven for 2 h at a temperature of 67° C. After recovery to room temperature, the sections were washed three times with PBS (pH7.4) for 5 min each time. Then, 50 μL 3% H₂O₂ was added and incubated at the room temperature for 30 minutes, and rinsed three times with PBS for 5 min each time. The sections were subsequently incubated with 0.5% Triton X-100 for 8 min at the room temperature, and rinsed three times with PBS for 5 min each time. Moreover, the sections were blocked with 5% goat serum for 60 min at room temperature, and then incubated with VDAC2 antibody (ab155803, 1:500, Abcam) overnight at 4° C, and rinsed three times with PBS for 5 min each time. Then, HRP-labeled Goat anti-rabbit IgG (ab7090, 1:8000, Abcam) was used to incubated

sections for 2 h, and rinsed three times with PBS. Finally, the sections were blocked with an anti-fluorescence quencher, and observed under a fluorescence microscope.

Transfection assay

Specific siRNAs targeting *VDAC2* (si-*VDAC2*) and control siRNA (si-NC) were purchased from Guangzhou RiboBio Co., Ltd. (Guangzhou, China). The A549 cells were inoculated in six-well plates and cultured at 37° C for 24 h with 5% CO₂. Subsequently, the cells were transfected with si-*VDAC2* and si-NC using Lipofectamine® 3000 (2343152, Invitrogen) at 37° C for 48 h according to the manufacturer's protocol. After 48 h transfection, qRT-PCR and western blotting were used to detect transfection efficiency.

Cell proliferation

The cell counting kit-8 (CCK-8) assay kit (AR1160-100, Boster Biological Technology., LTD, Wuhan, China) was used to analyze the cell proliferation capacity. Log phase cells were collected and the concentration of cell suspension was adjusted, and 100 μL cell suspensions were added into 96-well plates (2×10³ cells/well). Then the plates were pre-incubated in an incubator at 37° C with 5% CO₂. After 24 h, the 10 μL CCK-8 solution was added to each well and incubated for 1 h. The absorbance was measured with Microplate Reader (DNM-9602, Beijing Perlong Technology Co., Ltd, Beijing, China) at 450 nm.

Transwell migration assay

The transwell chamber was placed into a 24-well plate and coated with 100 μL Matrigel (300ug/mL) onto the compartment membrane, and the gel was placed in an incubator at 37° C for 3 h. The 200 μL cell suspensions (1~5×10⁵ cells/mL) were added to the upper chamber and 500 μL of complete medium was added to the lower chamber at 37° C and 5% CO₂ in the incubator for 24 h. Next, transwell chamber was washed twice with PBS and fixed with 4% paraformaldehyde for 30 min and stained with dye crystal violet solution for 30 min. The cells were washed with PBS and photographed using an inverted microscope (Olympus Corporation).

Clonogenic assay

The cells were seeded into 12 well microtiter plates at a density of 500 cells/well to a total volume of 200 μL per well, and incubated at 37° C in for 1 week. Then, the cells were washed with PBS (pH7.4), and were fixed with 1 mL 4% paraformaldehyde for 30 min, and washed

Table 1. Primer sequences for qPCR.

Target gene	Primer sequence
VDAC2-F	CGGAATTCATGGCGACCCACGGACAG
VDAC2-R	CTAGCTAGCAGCCTCCAACCTCCAGGGCG
β-actin-F	CCACGAAACTACCTTCAACTCC
β-actin-R	GTGATCTCCTTCTGCATCCTGT

with PBS. Next, the cells were stained with 1 mL of 0.1% crystal violet for 30 min, and rinsed with PBS. The plate was allowed to dry naturally and photographed. The number of colonies was obtained by analyzing the digital photographs of the plates, using the program ImageJ.

Statistical analysis

All bioinformatics data were analyzed using R software (Version 4.2.1). All experimental data were presented as mean ± standard deviation (SD). Data were analyzed using GraphPad Prism 6. Comparisons between multiple groups were made with one-way ANOVA, comparisons between two groups were performed by Independent-samples t test. The $p < 0.05$ was considered statistically significant.

Availability of data and materials

The datasets generated and analyzed during the current study are available from the Gene Expression Omnibus (GEO) datasets (<http://www.ncbi.nlm.nih.gov/geo>) and The Cancer Genome Atlas (TCGA, <https://tcga-data.nci.nih.gov/tcga/>) database.

Abbreviations

ICI: Immune checkpoint inhibitors; LUAD: Lung adenocarcinoma; LUSC: Lung squamous cell carcinoma; NSCLC: Non-small cell lung cancer; HRG: hypoxia related genes; TMB: Tumor mutational burden; VDAC: Voltage-dependent anion channel; OS: Overall Survival; EGFR: Epidermal growth factor receptor; TKI: Tyrosine kinase inhibitors; ROS: Reactive oxygen species; HIF: Hypoxia-inducible factor; EMT: Epithelial-mesenchymal transition; TME: Tumor microenvironment; ROC: Receiver operating characteristic; AUC: Area under the curve; CCK-8: Cell counting kit-8.

AUTHOR CONTRIBUTIONS

YM and BH contributed to the study conception and design. Data collection and analysis were performed by YM, QY and NZ. Validation was conducted by QY and NZ. The first draft of the manuscript was written by RY. All authors read and approved the final manuscript.

CONFLICTS OF INTEREST

The authors declare that there is no conflicts of interest regarding the publication of this article.

ETHICAL STATEMENT AND CONSENT

All experiments were approved by the Ethics Committee of the Affiliated People's Hospital of Inner Mongolia Medical University (ethic code: No. WZ202307), conformed to the declaration of Helsinki. The informed consent was obtained from all subjects.

FUNDING

The study was supported by the Inner Mongolia Natural Science Foundation [2023LHMS08029], the Construction Project of High-quality Clinical key Specialty for the Development of Public Hospitals in Inner Mongolia Autonomous region (Chest Tumor), Project Number: Document issued by the Health and Health Commission of Inner Mongolia Autonomous region (2023) No. 15, and 2022 Autonomous Region Health Science and Technology Plan Project [202201289, 202201363].

REFERENCES

1. Thai AA, Solomon BJ, Sequist LV, Gainor JF, Heist RS. Lung cancer. *Lancet*. 2021; 398:535–54. [https://doi.org/10.1016/S0140-6736\(21\)00312-3](https://doi.org/10.1016/S0140-6736(21)00312-3) PMID:34273294
2. Herbst RS, Morgensztern D, Boshoff C. The biology and management of non-small cell lung cancer. *Nature*. 2018; 553:446–54. <https://doi.org/10.1038/nature25183> PMID:29364287
3. Mithoowani H, Febbraro M. Non-Small-Cell Lung Cancer in 2022: A Review for General Practitioners in Oncology. *Curr Oncol*. 2022; 29:1828–39. <https://doi.org/10.3390/curroncol29030150> PMID:35323350
4. Massafra M, Passalacqua MI, Gebbia V, Macri P, Lazzari C, Gregorc V, Buda C, Altavilla G, Santarpia M. Immunotherapeutic Advances for NSCLC. *Biologics*. 2021; 15:399–417.

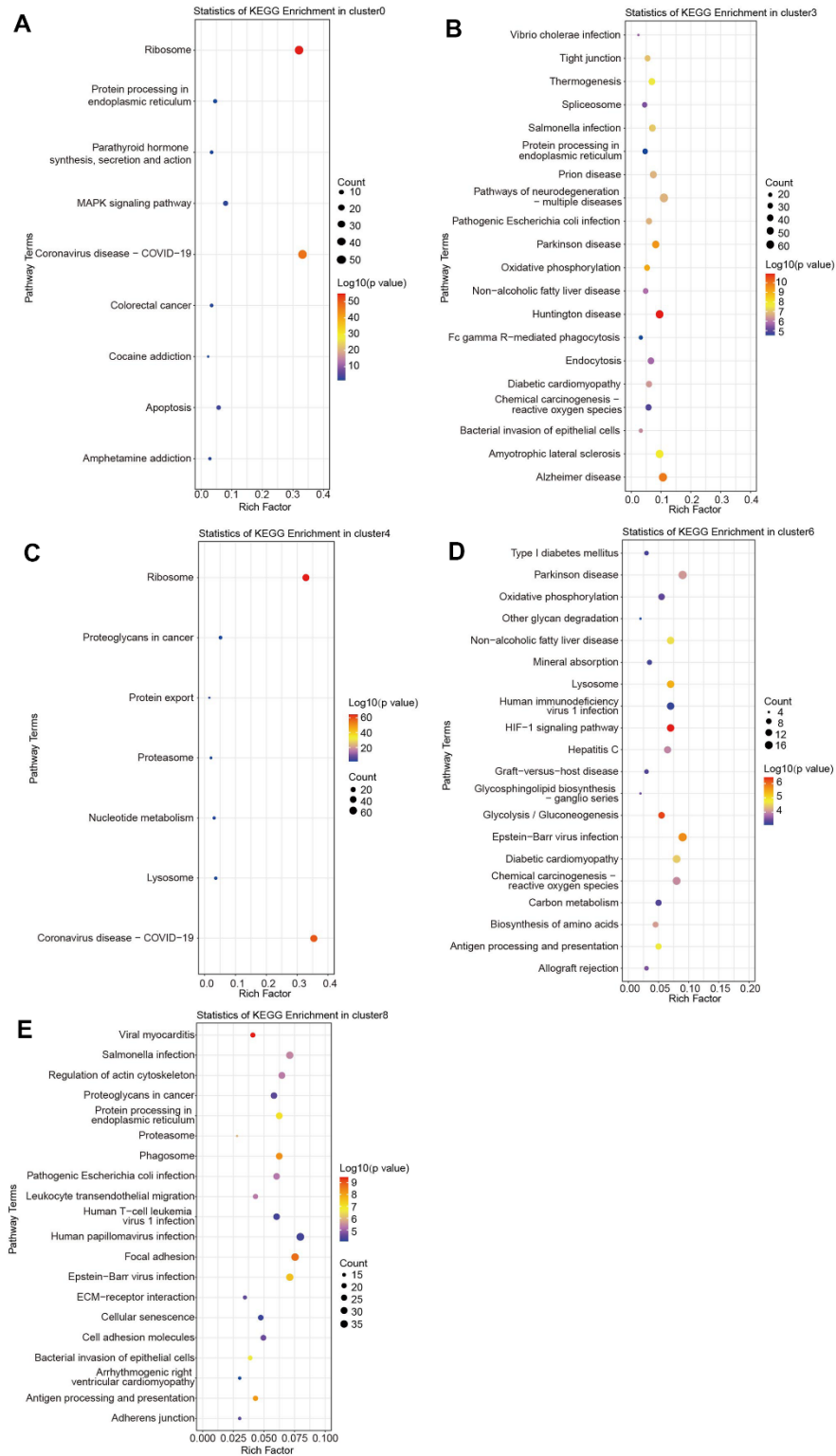
- <https://doi.org/10.2147/BTT.S295406>
PMID:34675481
5. Siegel RL, Miller KD, Jemal A. Cancer statistics, 2019. *CA Cancer J Clin.* 2019; 69:7–34.
<https://doi.org/10.3322/caac.21551>
PMID:30620402
 6. Lu Y, Ma T, Wang L, Xue T. [Advances in Lymph Node Metastasis and Lymph Node Dissection in Early Non-small Cell Lung Cancer]. *Zhongguo Fei Ai Za Zhi.* 2019; 22:520–5.
<https://doi.org/10.3779/j.issn.1009-3419.2019.08.07>
PMID:31451143
 7. Gibney GT, Weiner LM, Atkins MB. Predictive biomarkers for checkpoint inhibitor-based immunotherapy. *Lancet Oncol.* 2016; 17:e542–51.
[https://doi.org/10.1016/S1470-2045\(16\)30406-5](https://doi.org/10.1016/S1470-2045(16)30406-5)
PMID:27924752
 8. Eales KL, Hollinshead KE, Tennant DA. Hypoxia and metabolic adaptation of cancer cells. *Oncogenesis.* 2016; 5:e190.
<https://doi.org/10.1038/oncsis.2015.50>
PMID:26807645
 9. Harris B, Saleem S, Cook N, Searle E. Targeting hypoxia in solid and haematological malignancies. *J Exp Clin Cancer Res.* 2022; 41:318.
<https://doi.org/10.1186/s13046-022-02522-y>
PMID:36320041
 10. Ouyang W, Jiang Y, Bu S, Tang T, Huang L, Chen M, Tan Y, Ou Q, Mao L, Mai Y, Yao H, Yu Y, Lin X. A Prognostic Risk Score Based on Hypoxia-, Immunity-, and Epithelial-to-Mesenchymal Transition-Related Genes for the Prognosis and Immunotherapy Response of Lung Adenocarcinoma. *Front Cell Dev Biol.* 2022; 9:758777.
<https://doi.org/10.3389/fcell.2021.758777>
PMID:35141229
 11. Wu J, Li L, Zhang H, Zhao Y, Zhang H, Wu S, Xu B. A risk model developed based on tumor microenvironment predicts overall survival and associates with tumor immunity of patients with lung adenocarcinoma. *Oncogene.* 2021; 40:4413–24.
<https://doi.org/10.1038/s41388-021-01853-y>
PMID:34108619
 12. Wang DD, Shaver LG, Shi FY, Wei JJ, Qin TZ, Wang SZ, Kong YJ. Comparative efficacy and safety of PD-1/PD-L1 immunotherapies for non-small cell lung cancer: a network meta-analysis. *Eur Rev Med Pharmacol Sci.* 2021; 25:2866–84.
https://doi.org/10.26355/eurev_202104_25541
PMID:33877652
 13. Lu Y, Liu Y, Oeck S, Zhang GJ, Schramm A, Glazer PM. Hypoxia Induces Resistance to EGFR Inhibitors in Lung Cancer Cells via Upregulation of FGFR1 and the MAPK Pathway. *Cancer Res.* 2020; 80:4655–67.
<https://doi.org/10.1158/0008-5472.CAN-20-1192>
PMID:32873635
 14. Hao S, Zhu X, Liu Z, Wu X, Li S, Jiang P, Jiang L. Chronic intermittent hypoxia promoted lung cancer stem cell-like properties via enhancing Bach1 expression. *Respir Res.* 2021; 22:58.
<https://doi.org/10.1186/s12931-021-01655-6>
PMID:33596919
 15. Kong X, Zhao Y, Li X, Tao Z, Hou M, Ma H. Overexpression of HIF-2 α -Dependent NEAT1 Promotes the Progression of Non-Small Cell Lung Cancer through miR-101-3p/SOX9/Wnt/ β -Catenin Signal Pathway. *Cell Physiol Biochem.* 2019; 52:368–81.
<https://doi.org/10.33594/000000026>
PMID:30845377
 16. Chen X, Wang P, Guo F, Wang X, Wang J, Xu J, Yuan D, Zhang J, Shao C. Autophagy enhanced the radioresistance of non-small cell lung cancer by regulating ROS level under hypoxia condition. *Int J Radiat Biol.* 2017; 93:764–70.
<https://doi.org/10.1080/09553002.2017.1325025>
PMID:28463025
 17. Yamamoto T, Yamada A, Watanabe M, Yoshimura Y, Yamazaki N, Yoshimura Y, Yamauchi T, Kataoka M, Nagata T, Terada H, Shinohara Y. VDAC1, having a shorter N-terminus than VDAC2 but showing the same migration in an SDS-polyacrylamide gel, is the predominant form expressed in mitochondria of various tissues. *J Proteome Res.* 2006; 5:3336–44.
<https://doi.org/10.1021/pr060291w> PMID:17137335
 18. Colombini M. VDAC: the channel at the interface between mitochondria and the cytosol. *Mol Cell Biochem.* 2004; 256–7:107–15.
<https://doi.org/10.1023/b:mcbi.0000009862.17396.8d>
PMID:14977174
 19. Shoshan-Barmatz V, Ben-Hail D. VDAC, a multi-functional mitochondrial protein as a pharmacological target. *Mitochondrion.* 2012; 12:24–34.
<https://doi.org/10.1016/j.mito.2011.04.001>
PMID:21530686
 20. Józwiak P, Ciesielski P, Forma E, Kozal K, Wójcik-Krowiranda K, Cwonda Ł, Bieńkiewicz A, Bryś M, Krześlak A. Expression of voltage-dependent anion channels in endometrial cancer and its potential prognostic significance. *Tumour Biol.* 2020; 42:1010428320951057.
<https://doi.org/10.1177/1010428320951057>
PMID:32829673
 21. Zhou K, Yao YL, He ZC, Chen C, Zhang XN, Yang KD, Liu YQ, Liu Q, Fu WJ, Chen YP, Niu Q, Ma QH, Zhou R, et al.

- VDAC2 interacts with PFKP to regulate glucose metabolism and phenotypic reprogramming of glioma stem cells. *Cell Death Dis.* 2018; 9:988.
<https://doi.org/10.1038/s41419-018-1015-x>
PMID:30250190
22. Chin HS, Li MX, Tan IKL, Ninnis RL, Reljic B, Scicluna K, Dagley LF, Sandow JJ, Kelly GL, Samson AL, Chappaz S, Khaw SL, Chang C, et al. VDAC2 enables BAX to mediate apoptosis and limit tumor development. *Nat Commun.* 2018; 9:4976.
<https://doi.org/10.1038/s41467-018-07309-4>
PMID:30478310
23. Wang Z, Qin J, Zhao J, Li J, Li D, Popp M, Popp F, Alakus H, Kong B, Dong Q, Nelson PJ, Zhao Y, Bruns CJ. Inflammatory IFIT3 renders chemotherapy resistance by regulating post-translational modification of VDAC2 in pancreatic cancer. *Theranostics.* 2020; 10:7178–92.
<https://doi.org/10.7150/thno.43093>
PMID:32641986
24. Yang Y, Luo M, Zhang K, Zhang J, Gao T, Connell DO, Yao F, Mu C, Cai B, Shang Y, Chen W. Nedd4 ubiquitylates VDAC2/3 to suppress erastin-induced ferroptosis in melanoma. *Nat Commun.* 2020; 11:433.
<https://doi.org/10.1038/s41467-020-14324-x>
PMID:31974380
25. Stankovic B, Bjørhovde HAK, Skarshaug R, Aamodt H, Frafjord A, Müller E, Hammarström C, Beraki K, Bækkevold ES, Woldbæk PR, Helland Å, Brustugun OT, Øynebråten I, Corthay A. Immune Cell Composition in Human Non-small Cell Lung Cancer. *Front Immunol.* 2019; 9:3101.
<https://doi.org/10.3389/fimmu.2018.03101>
PMID:30774636
26. Schalper KA, Brown J, Carvajal-Hausdorf D, McLaughlin J, Velcheti V, Syrigos KN, Herbst RS, Rimm DL. Objective measurement and clinical significance of TILs in non-small cell lung cancer. *J Natl Cancer Inst.* 2015; 107:dju435.
<https://doi.org/10.1093/jnci/dju435> PMID:25650315
27. Obeid JM, Wages NA, Hu Y, Deacon DH, Slingluff CL Jr. Heterogeneity of CD8+ tumor-infiltrating lymphocytes in non-small-cell lung cancer: impact on patient prognostic assessments and comparison of quantification by different sampling strategies. *Cancer Immunol Immunother.* 2017; 66:33–43.
<https://doi.org/10.1007/s00262-016-1908-4>
PMID:27770170
28. Gentles AJ, Newman AM, Liu CL, Bratman SV, Feng W, Kim D, Nair VS, Xu Y, Khuong A, Hoang CD, Diehn M, West RB, Plevritis SK, Alizadeh AA. The prognostic landscape of genes and infiltrating immune cells across human cancers. *Nat Med.* 2015; 21:938–45.
<https://doi.org/10.1038/nmeth.3337>
PMID:25822800
29. Lee YS, Radford KJ. The role of dendritic cells in cancer. *Int Rev Cell Mol Biol.* 2019; 348:123–78.
<https://doi.org/10.1016/bs.ircmb.2019.07.006>
PMID:31810552
30. Goc J, Germain C, Vo-Bourgais TK, Lupo A, Klein C, Knockaert S, de Chaisemartin L, Ouakrim H, Becht E, Alifano M, Validire P, Remark R, Hammond SA, et al. Dendritic cells in tumor-associated tertiary lymphoid structures signal a Th1 cytotoxic immune contexture and license the positive prognostic value of infiltrating CD8+ T cells. *Cancer Res.* 2014; 74:705–15.
<https://doi.org/10.1158/0008-5472.CAN-13-1342>
PMID:24366885
31. Yarchoan M, Hopkins A, Jaffee EM. Tumor Mutational Burden and Response Rate to PD-1 Inhibition. *N Engl J Med.* 2017; 377:2500–1.
<https://doi.org/10.1056/NEJMc1713444>
PMID:29262275
32. Hellmann MD, Ciuleanu TE, Pluzanski A, Lee JS, Otterson GA, Audigier-Valette C, Minenza E, Linardou H, Burgers S, Salman P, Borghaei H, Ramalingam SS, Brahmer J, et al. Nivolumab plus Ipilimumab in Lung Cancer with a High Tumor Mutational Burden. *N Engl J Med.* 2018; 378:2093–104.
<https://doi.org/10.1056/NEJMoa1801946>
PMID:29658845
33. Rizvi H, Sanchez-Vega F, La K, Chatila W, Jonsson P, Halpenny D, Plodkowski A, Long N, Sauter JL, Rekhtman N, Hollmann T, Schalper KA, Gainor JF, et al. Molecular Determinants of Response to Anti-Programmed Cell Death (PD)-1 and Anti-Programmed Death-Ligand 1 (PD-L1) Blockade in Patients With Non-Small-Cell Lung Cancer Profiled With Targeted Next-Generation Sequencing. *J Clin Oncol.* 2018; 36:633–41.
<https://doi.org/10.1200/JCO.2017.75.3384>
PMID:29337640
34. Yoshihara K, Shahmoradgoli M, Martínez E, Vegesna R, Kim H, Torres-Garcia W, Treviño V, Shen H, Laird PW, Levine DA, Carter SL, Getz G, Stemke-Hale K, et al. Inferring tumour purity and stromal and immune cell admixture from expression data. *Nat Commun.* 2013; 4:2612.
<https://doi.org/10.1038/ncomms3612>
PMID:24113773
35. Newman AM, Liu CL, Green MR, Gentles AJ, Feng W, Xu Y, Hoang CD, Diehn M, Alizadeh AA. Robust enumeration of cell subsets from tissue expression profiles. *Nat Methods.* 2015; 12:453–7.
<https://doi.org/10.1038/nmeth.3337>
PMID:25822800

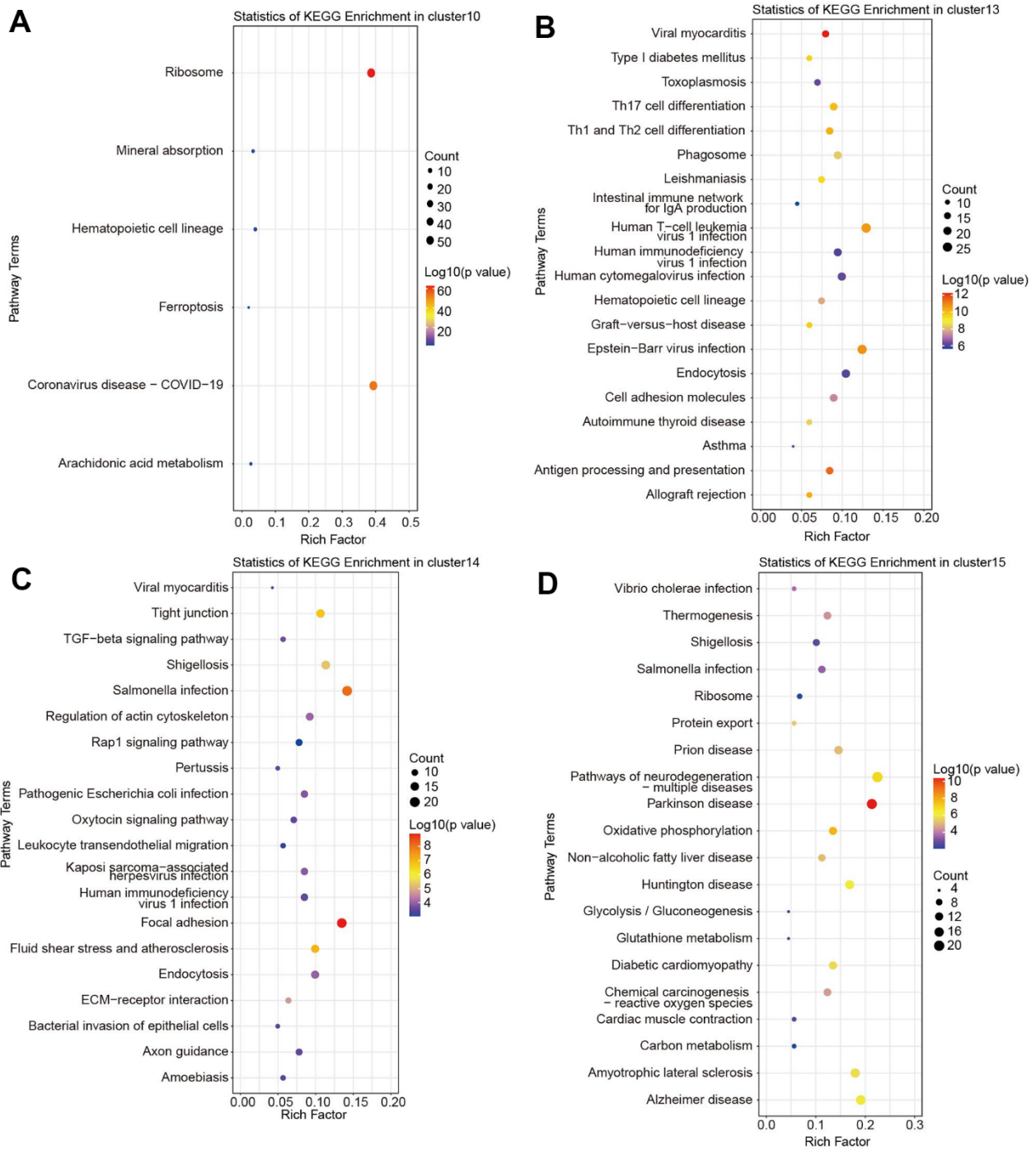
36. Li L, Li S. miR-205-5p inhibits cell migration and invasion in prostatic carcinoma by targeting ZEB1. *Oncol Lett.* 2018; 16:1715–21.
<https://doi.org/10.3892/ol.2018.8862>
PMID:[30008858](https://pubmed.ncbi.nlm.nih.gov/30008858/)

SUPPLEMENTARY MATERIALS

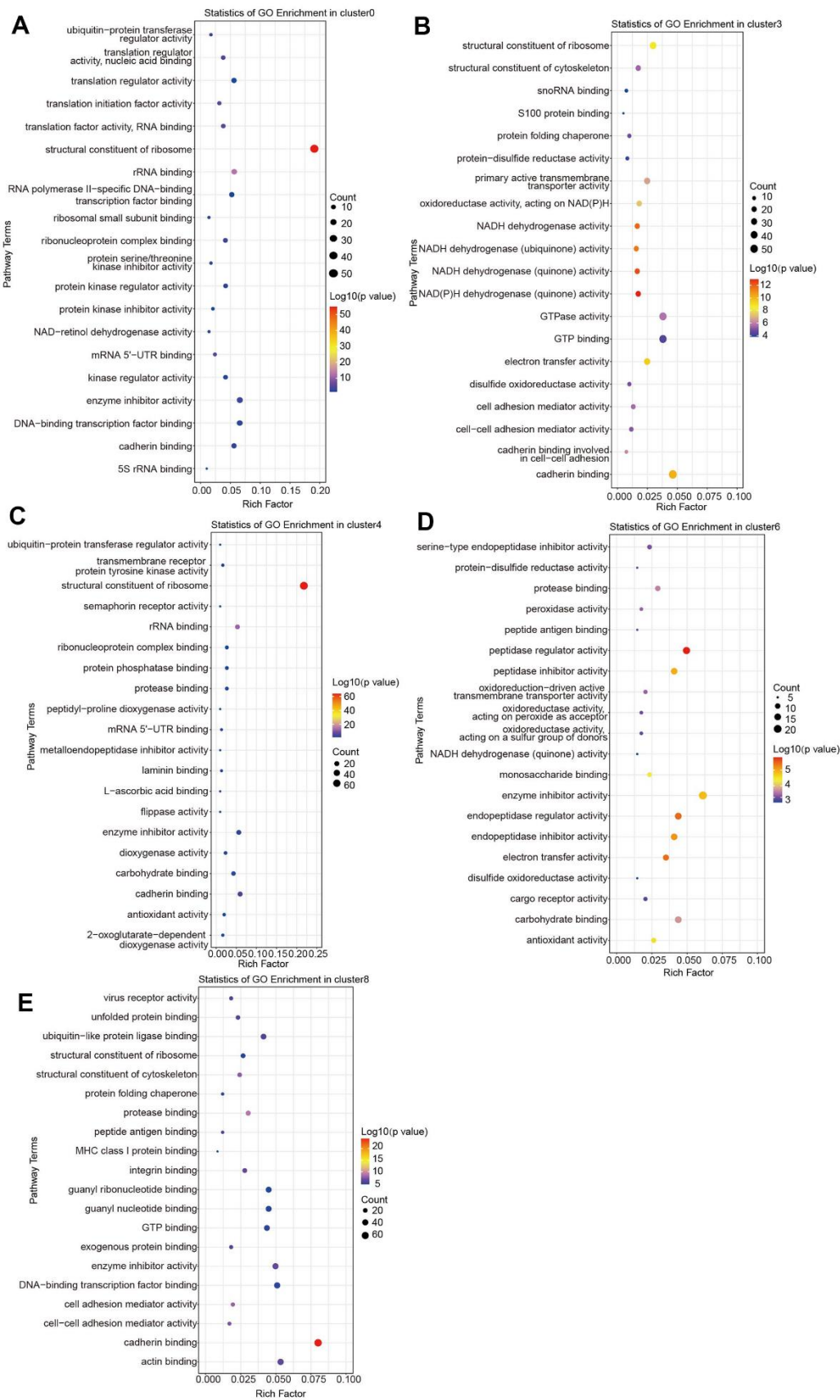
Supplementary Figures



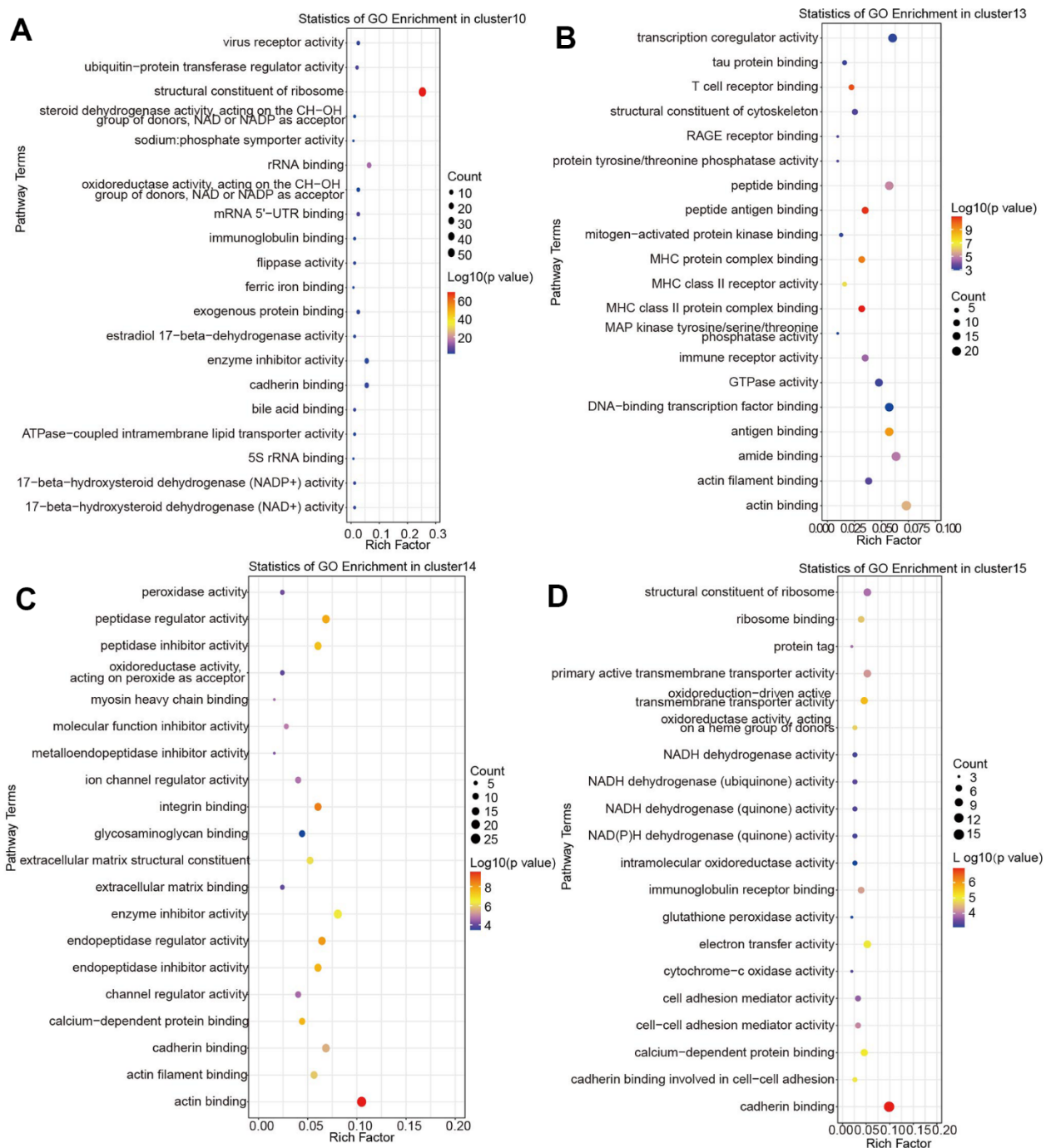
Supplementary Figure 1. The results of KEGG enriched analysis in cluster0 (A), cluster3 (B), cluster4 (C), cluster6 (D) and cluster8 (E).



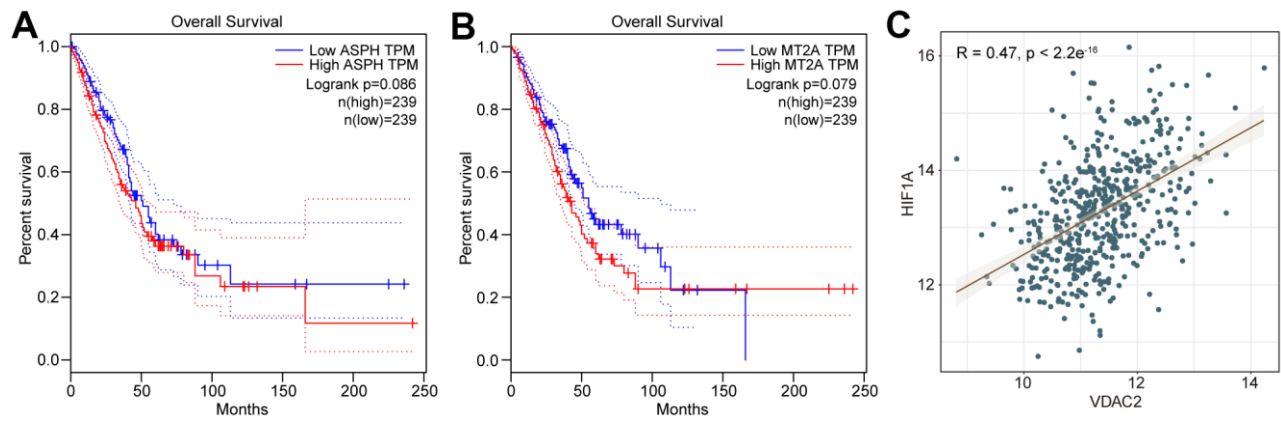
Supplementary Figure 2. The results of KEGG enriched analysis in cluster10 (A), cluster13 (B), cluster14 (C) and cluster15 (D).



Supplementary Figure 3. The results of GO enriched analysis in cluster0 (A), cluster3 (B), cluster4 (C), cluster6 (D) and cluster8 (E).



Supplementary Figure 4. The results of GO enriched analysis in cluster10 (A), cluster13 (B), cluster14 (C) and cluster15 (D).



Supplementary Figure 5. The overall survival rate of patients with high or low *ASPH* (A) and *MT2A* (B) expression. (C) The correlation between *VDAC2* expression and hypoxia-inducible factor 1- α (HIF-1 α).

Supplementary Tables

Supplementary Table 1. Prognosis associated genes between C1 and C2 groups.

Gene	HR	z	P-value	Lower	Upper
LDHA	1.360890939	3.707311499	0.000209471	1.156309886	1.601667659
GAPDH	1.311404491	3.57007769	0.000356875	1.130054847	1.521856875
TPI1	1.230060274	2.335626069	0.019510739	1.033864827	1.463487527
VDAC2	1.214727042	1.977002413	0.048041357	1.001677835	1.473090183
ALDOA	1.209959033	2.281359892	0.022527159	1.027213353	1.425215957
CTSL	1.178130335	2.811213704	0.004935499	1.050891073	1.320775409
MIF	1.174266645	2.177645446	0.029432443	1.01618788	1.356936234
PLAUR	1.145686306	2.284546906	0.022339409	1.019510999	1.287477147
ERRFI1	1.144607836	2.30380039	0.021233851	1.020362213	1.283982375
ASPH	1.134771595	2.312315735	0.02076029	1.019452455	1.263135487
MT2A	1.11485957	2.044269965	0.040926885	1.004494045	1.23735115
SCGB1A1	0.957232918	-2.496704198	0.012535347	0.924945346	0.99064757
SFTPC	0.951924195	-3.082844116	0.002050325	0.922568243	0.982214248
AQP5	0.950860677	-2.394798961	0.01662948	0.912446049	0.990892588
SCGB3A2	0.948836286	-2.632648622	0.008472195	0.912453137	0.986670177
PIGR	0.943784359	-2.540433142	0.011071526	0.902582536	0.986866996
SCGB3A1	0.933044378	-3.340134876	0.000837377	0.895862206	0.971769772
CCL19	0.93144917	-2.037018444	0.041648194	0.869931265	0.997317365
IGHA1	0.925143464	-2.027833339	0.04257726	0.858122155	0.997399291
FOLR1	0.923837419	-2.665116957	0.007696155	0.871553474	0.979257845
IGKC	0.923072168	-2.202464509	0.027632513	0.859605156	0.991225123
SLC22A31	0.919273438	-2.949283292	0.003185119	0.86926396	0.972160002
C4BPA	0.917551185	-3.465879222	0.000528501	0.873972233	0.963303117
SFTA1P	0.914684476	-2.882207165	0.003949	0.860864799	0.971868859
C7	0.913936967	-2.854753547	0.004307024	0.859177392	0.972186638
SFTPB	0.911886553	-4.239856378	2.24E-05	0.873821241	0.951610061
SFTPD	0.909237414	-3.544634867	0.000393157	0.862637628	0.958354526
C16orf89	0.907997902	-3.837446851	0.00012432	0.864324474	0.953878103
NAPSA	0.906894162	-4.10130205	4.11E-05	0.865512626	0.950254215
AQP3	0.906421516	-2.681734804	0.00732415	0.843615789	0.973903021
IGLC3	0.903923499	-2.777570168	0.005476701	0.841737049	0.970704204
RGS1	0.902500596	-2.008603703	0.044579178	0.816533231	0.997518894
DCN	0.898596825	-2.026246759	0.042739504	0.810305431	0.996508506
HLA-DQB1	0.892443129	-2.699060479	0.006953554	0.821663248	0.969320144
GDF15	0.887924503	-2.8459562	0.004427828	0.818132143	0.963670637
IL7R	0.887066616	-2.420111186	0.015515762	0.805022091	0.977472781
TRAC	0.885218608	-2.124717296	0.033610209	0.79105529	0.990590664
TRBC2	0.885124367	-2.171268029	0.029910918	0.792804386	0.988194767
HLA-DRB5	0.884982441	-3.061262949	0.002204054	0.818388905	0.956994793
HLA-DPA1	0.884854804	-2.594201323	0.009481095	0.806738717	0.970534832
LTB	0.883876998	-2.522370393	0.01165669	0.803038818	0.972852782
SPARCL1	0.882290731	-2.183385667	0.029007421	0.788476734	0.987266841
CXCL17	0.879437443	-4.576053762	4.74E-06	0.832352798	0.929185579
LST1	0.87873819	-2.369291868	0.017822183	0.789619834	0.977914653
MS4A7	0.878056597	-2.39953259	0.016416018	0.78957082	0.976458815
CYB5A	0.877396939	-2.253662039	0.024217437	0.783059806	0.983099097
A2M	0.876367584	-2.350669233	0.018739684	0.785052556	0.97830411
MFAP4	0.875952513	-3.015423202	0.002566209	0.803700233	0.95470024
CD79A	0.875236415	-3.363419537	0.000769833	0.809841682	0.945911774
HLA-DRB1	0.874978348	-2.7879849	0.005303702	0.796564948	0.961110718
SFTA3	0.874968709	-4.957668635	7.13E-07	0.829965145	0.922412521

SOD3	0.873822967	-2.512205712	0.011997913	0.786544699	0.970785994
ACP5	0.873398978	-2.059267081	0.03946866	0.767821436	0.993493719
TSTD1	0.872882353	-1.979854526	0.047719877	0.762964996	0.99863507
HLA-DQA1	0.872548687	-3.01019349	0.002610813	0.798430819	0.953546874
CD74	0.871151342	-2.760652055	0.00576861	0.789882007	0.960782312
HLA-DRA	0.870665571	-2.854035064	0.004316777	0.791671919	0.957541272
CD3D	0.869754364	-2.535314672	0.011234636	0.780811569	0.968828696
CD48	0.869151053	-2.609124888	0.009077411	0.782246932	0.965709831
TSC22D3	0.868276687	-2.231458122	0.025650799	0.766972058	0.982962022
WFDC2	0.865746406	-3.525547716	0.000422608	0.799068842	0.937987817
HLA-DPB1	0.865639757	-2.931664764	0.003371505	0.786038805	0.953301777
IFT57	0.864129833	-2.397057713	0.01652732	0.766871432	0.973723022
CD37	0.864018055	-2.565435951	0.010304624	0.772728572	0.9660924
RNASE1	0.86325175	-3.302698273	0.000957594	0.791113288	0.941968231
BCAM	0.862131242	-2.664016675	0.007721374	0.772989487	0.961552895
PTGDS	0.861585425	-3.315587512	0.000914507	0.788952486	0.940905135
CD69	0.861299386	-2.906354643	0.003656667	0.778796352	0.952542511
HNMT	0.856921261	-2.304196835	0.021211597	0.751449934	0.977196235
HLA-DMB	0.854469141	-3.03274766	0.002423382	0.771887532	0.945885874
WSB1	0.852954777	-2.600305038	0.009314093	0.756592281	0.961590371
SNHG7	0.849665238	-2.273041308	0.023023691	0.738313395	0.977811078
NUPR1	0.848438019	-2.911106298	0.003601515	0.759560035	0.947715834
ID2	0.84258859	-2.347495228	0.018900115	0.730315876	0.972121181
CXCR4	0.842309652	-2.607587163	0.009118285	0.740377932	0.958274849
MGP	0.841554756	-3.26310677	0.00110198	0.758723601	0.933428729
LTA4H	0.840710894	-2.086643419	0.036920379	0.714279236	0.989521704
TRBC1	0.837212032	-3.285221497	0.001019022	0.753007112	0.930833157
TMSB4X	0.833258015	-2.299083481	0.021500199	0.713253948	0.973452612
CD47	0.830496348	-2.424255386	0.015339814	0.714700073	0.965054028
EPHX1	0.828418415	-3.51881723	0.000433475	0.745959504	0.919992394
ALDH2	0.826400318	-2.974475226	0.002934902	0.728827901	0.93703532
ASAH1	0.823374798	-2.436539778	0.014828538	0.704212712	0.962700681
HLA-DMA	0.823143292	-3.491285992	0.000480701	0.737945727	0.918177117
ATP6V0D1	0.822638322	-2.070159278	0.038437431	0.683803519	0.989661197
CTSZ	0.822143977	-2.46294847	0.013779972	0.703501686	0.960794739
SSR4	0.820126991	-2.39091454	0.016806464	0.697083361	0.964889308
NPC2	0.818435795	-3.507431274	0.000452455	0.731745627	0.915396178
VAMP8	0.816019376	-2.364851588	0.018037298	0.689475368	0.965788849
CTSH	0.815403585	-3.791665484	0.00014964	0.733769919	0.906119191
COX14	0.814171368	-2.16454563	0.030422499	0.675881142	0.980756787
C14orf28	0.811471679	-1.99542611	0.045996426	0.660935533	0.996294271
KLRB1	0.811261893	-3.496017517	0.000472258	0.721496564	0.912195417
FBP1	0.809136416	-3.522662073	0.000427236	0.719194285	0.910326671
SMDT1	0.80182364	-2.328189804	0.019902027	0.66577667	0.96567089
FCGRT	0.783363551	-3.180936097	0.001468	0.673950311	0.91053961
HMG3	0.782802046	-3.044670394	0.002329354	0.668639276	0.916456848
CIRBP	0.7817752	-2.967341056	0.003003875	0.664448321	0.919819411
ISCU	0.755610674	-2.501133314	0.012379657	0.606636824	0.941168535
AKR1A1	0.749640083	-2.631956588	0.008489471	0.604864718	0.929067671
PEBP1	0.745189336	-3.066893752	0.002162957	0.61749848	0.899285043

Supplementary Table 2. The clinical features of NSCLC patients.

Sex	Age	Tumor size (cm×cm×cm)	T	N	M	Differentiation grade
Male	45	2.5*2*1.5	4	2	1a	medium-low differentiated adenocarcinoma
Female	56	3.5*3*3	2a	2	0	medium-low differentiated adenocarcinoma
Male	62	5*4.5*4	3	1	0	medium-differentiated adenocarcinoma
Female	66	3.1*2.6*2.2	3	0	0	medium-differentiated adenocarcinoma
Female	57	4.5*3.5*3	2b	2	0	medium-differentiated adenocarcinoma
Male	56	6.5*4*4	3	0	0	poorly differentiated adenocarcinoma
Male	50	1*1*0.3+1.5*1*0.5	3	1	1a	poorly differentiated adenocarcinoma
Female	48	1.1*0.9*0.3	1b	0	0	highly differentiated adenocarcinoma
Female	68	1*1*0.7	2a	0	0	medium-differentiated adenocarcinoma
Female	59	4.2*4.5*2.6	2b	0	0	medium-differentiated adenocarcinoma
Female	55	2*1.5*1	2a	0	0	medium-differentiated adenocarcinoma
Male	59	3.7*3.3*1.7	2a	2	0	medium-low differentiated adenocarcinoma
Male	68	5*3.5*2	2b	0	0	medium-low differentiated adenocarcinoma
Female	60	2.6*1.8*1.5	2a	0	0	medium-differentiated adenocarcinoma
Male	58	1.3*0.6*0.6	1b	0	0	highly differentiated adenocarcinoma